Mechanical Design and development of a new version of Multi-Modal Mobility Morphobot (M4)

A Thesis Presented
by

Dharsan Krishnamoorthy

to

The Department of Mechanical and Industrial Engineering

in partial fulfillment of the requirements
for the degree of

Master of Science

in

Robotics

Northeastern University
Boston, Massachusetts

April 2025

Contents

List of Figures

List of Tables

Acknowledgments

I extend my sincere gratitude to all the members of the Silicon Synapse Lab at Northeastern University for their support throughout my thesis journey. I am especially grateful to Prof. Alireza Ramezani and Prof. Rifat Sipahi, my primary and co-advisors, respectively, for their technical guidance, mentorship, and continuous encouragement. Their insights played a pivotal role in shaping both the direction and depth of this work.

I would also like to acknowledge Adarsh Salagame (Ph.D. candidate) for his extensive support in setting up the robot's control architecture and electronics, and for his valuable feedback during the writing and presentation phases of this thesis. I am thankful to Yogi Shah (M.S. student) for his assistance with 3D printing and wiring, which accelerated the prototyping process and brought mechanical components to life.

Special thanks are due to both Adarsh Salagame and Prof. Ramezani for their guidance in drafting this thesis and preparing the final defense presentation.

Lastly, I am deeply grateful to my parents, whose moral and financial support enabled me to pursue my graduate education at Northeastern University. Their belief in me has been the foundation of this accomplishment.

Abstract

Mechanical Design and development of a new version of Multi-Modal Mobility Morphobot (M4)

by

Dharsan Krishnamoorthy

Master of Science in Robotics

Northeastern University, April 2025

Dr. Alireza Ramezani, Adviser

This thesis presents the complete design, fabrication, and experimental validation of a new version of Multi-Modal Mobility Morphobot (M4), a robotic system capable of transitioning between wheeled, aerial, and morphing locomotion, which was reported in July 2023. Developed to operate in extreme environments such as planetary terrains and disaster zones, the M4 robot embodies a unified design philosophy centered on appendage repurposing, structural morphing, and energy-efficient autonomy. This thesis specifically targets a fully embedded hardware architecture, leveraging 3D-printed structural components, modular assemblies, and integrated actuation via servo motors and BLDC-driven propellers. The system is designed to support multiple operational modes—including chassis bridging, flattening, dynamic balancing, and morphing flight—enabled through coordinated reconfiguration of shared appendages. This work also aims to address core challenges in scalability, robustness, and redundancy manipulation in the original design.

Chapter 1

Introduction

1.1 Background and Motivation

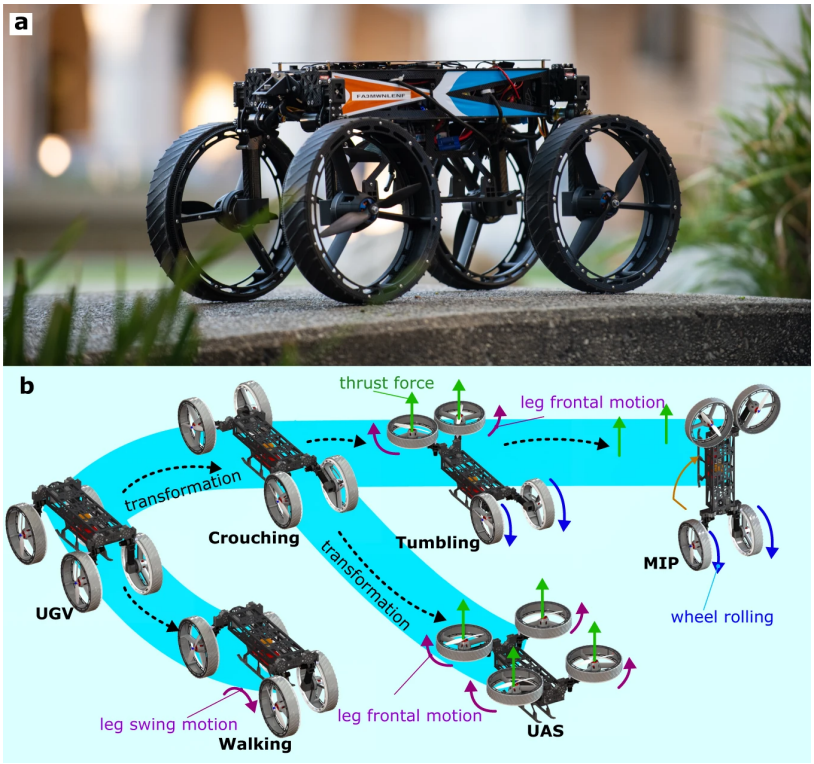

Figure 1.1: a) Shows M4 in wheeled mode. b) Illustrates cartoon depictions of M4's transformation to other modes [1].

In recent years, there has been a notable surge in interest surrounding robotic technologies

for space exploration, with particular emphasis on missions to Mars. This growing fascination has catalyzed the emergence of a wide array of innovative mobility platforms, each aimed at tackling the extreme and unpredictable conditions present on planetary surfaces. NASA and the Jet Propulsion Laboratory (JPL), leveraging their long-standing legacy of robotic exploration, have spearheaded several landmark missions using platforms such as the *Spirit*, *Opportunity*, and *Curiosity* rovers. These efforts have been pivotal in expanding humanity's understanding of Mars, while simultaneously highlighting the limitations of traditional wheeled systems in navigating complex terrain.

More recently, the deployment of the *Perseverance* rover marked a significant step forward, both in terms of scientific instrumentation and system complexity. This platform, carrying onboard the *Ingenuity* helicopter—a historic aerial scout—demonstrated the utility of augmenting ground mobility with aerial reconnaissance. However, the increased sophistication and mass of such platforms, along with the integration of multiple distinct systems, have caused mission costs to escalate substantially. Moreover, despite their engineering advances, these systems remain constrained by the harsh and highly variable topographies they must traverse [1].

To address these constraints, our research community initiated a line of investigation into robots capable of exhibiting *multi-modal locomotion*, capable of adapting their morphology and control to distinct operational needs. The first efforts centered around integrating small-scale thrusters into legged robots to augment locomotion and enhance versatility on uneven or unstructured surfaces. This work, referred to as *thruster-assisted legged mobility*, was proposed as a strategy for overcoming gravitational and topographical limitations on Mars [2]. It was subsequently expanded to include methods for regulating ground contact forces in quadrupedal systems to ensure stable and dynamically feasible gaits [3].

These foundational studies culminated in the design and prototyping of Harpy, a bipedal robot that incorporated aerial thrusters to assist with stability, posture control, and recovery. Harpy marked a major breakthrough in dynamic locomotion, demonstrating controlled thruster-assisted bipedal walking and flying transitions [4]–[11]. Building on this architecture, the research team introduced the Husky Carbon platform—a quadrupedal aerial-leg hybrid robot that further demonstrated multi-modal navigation with real-time autonomy [12], [13].

Alongside these developments, the broader vision of *morpho-functional robots*—machines capable of morphing their structure to support both terrestrial and aerial movement—began to take form [14]. This vision inspired new directions, such as enabling inclined surface walking through structural adaptation [15], and the construction of scalable unmanned ground-aerial hybrid robots capable of autonomously generating and executing 3D paths [16]. These ideas were further con-

solidated into the concept of the Multi-Modal Mobility Unmanned Vehicle, which seamlessly combined thruster-assisted legged locomotion with aerial capabilities into a single system [17], laying the groundwork for efficient aerial mobility solutions designed specifically for Mars exploration [18].

Modality	**Pros**	**Cons**
Wheeled	Fast Low energy consumption Naturally stable Large payload capacity	Only ground locomotion No obstacles overcome Subject to the terrain conditions
Legged	Can overcome small obstacles Efficient Agile Medium payload capacity	Slow Cannot overcome high obstacles Need to keep balance Subject to the terrain conditions
Aerial	Fast Agile 3D locomotion Can overcome almost all kinds of obstacles	High energy consumption Small autonomy Light robots with small payload Subject to aerodynamic constraints (wind, ground effects...) Noisy

Table 1.1: Various advantages and disadvantages of different locomotion modes [19].

Building upon this extensive and evolving body of work, the concept of the M4 robot emerged. This platform represents a significant departure from conventional modular robots by aiming to unify multiple locomotion modes—wheeled, legged, and aerial—into a single morphing structure. Drawing inspiration from biology, where animals repurpose their limbs for different functions (e.g., birds use wings for flying and perching), the M4 platform is bio-inspired both in form and function. The key novelty of M4 lies in its ability to *morph*—reconfiguring its structure in real-time to support diverse operational modes (see Figure 1.3). While existing multi-modal robots (Figure 1.2) typically rely on distinct appendages for each task, M4 achieves redundancy and efficiency by employing shared mechanical structures capable of reconfiguration.

Despite the added complexity in both hardware integration and control design, the M4's compactness, embeddedness, and versatility make it an exceptionally promising candidate for future planetary and terrestrial missions. For example, whereas traditional rovers must deploy a separate drone to access craters or elevated regions, the M4 can morph and fly autonomously into and out of such locations. In search and rescue contexts, its ability to transition between wheeled navigation,

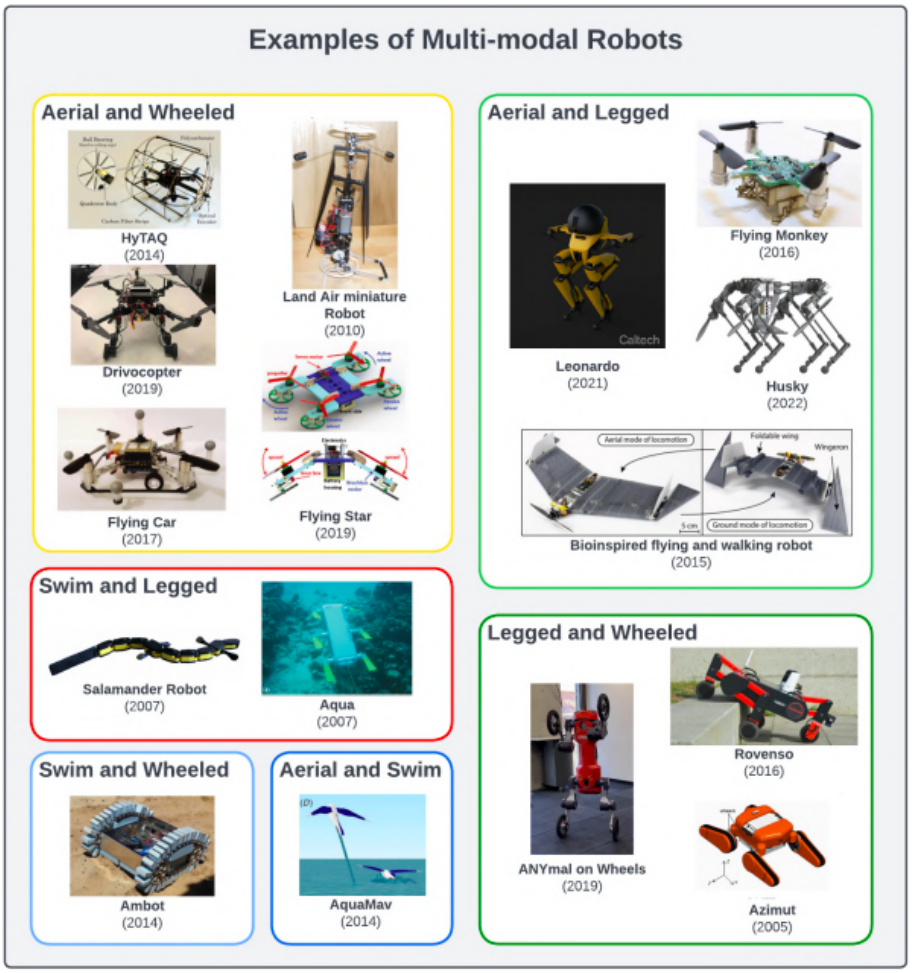

Figure 1.2: Examples of multi-modal robots [20]–[29].

aerial lift, and narrow-profile crawling could prove invaluable in accessing collapsed or otherwise inaccessible areas [1].

The morphing capability also offers an expanded operational envelope that single-mode robots cannot match. The M4 can traverse long distances efficiently as a rover, perform high-agility postural maneuvers as a Segway-style balancer, and take flight as needed to overcome impassable obstacles—see Figure 1.3 [1]. While the current prototype is an early version assembled under tight time constraints, it demonstrates the feasibility and advantages of fully embedded morphing architectures. Some mechatronic design limitations remain, such as limited onboard space for additional payloads or modules, requiring external mounting of new components [19], [30]. However, these challenges are a natural consequence of compact integration and do not hinder further development

of its autonomy stack or structural refinements.

The development of Multi-Modal Mobility Morphobot (M4) builds upon extensive prior research within the Silicon Synapse Lab, exploring morphing structures and multi-modal locomotion capabilities inspired by biological systems. The foundational concepts emerged from earlier studies in thruster-assisted legged locomotion, as demonstrated by Harpy which established the potential for integrating thrust vectoring to augment legged mobility. Further enhancements in thruster-assisted methods were explored to achieve robust locomotion on uneven terrains, addressing real-time gait feasibility constraints [31]–[37]

M4 specifically integrates appendage repurposing, significantly inspired by studies of biologically informed morphing structures and aerodynamic modeling from the lab. Notably, morphing wing dynamics investigated through lifting line theory and Wagner's function provided critical aerodynamic insights. These studies informed the robot's capability for morphing flight and dynamic structural adaptation to aerodynamic conditions, enabling agility and fault tolerance. [38]–[45]

The research direction of employing multi-functional appendages to enhance locomotion versatility has its roots in pioneering projects like LEONARDO, a synchronized multi-modal robot capable of aerial and legged locomotion, and the Husky Carbon platform, a morpho-functional legged-aerial robot demonstrating real-time multi-modal navigation. Further, platforms like COBRA explored integrated dynamics and obstacle avoidance through dynamic posture manipulation and slithering motions, advancing contact-implicit motion planning methods. [46]–[51]

Critical foundational research in autonomous 3D path planning was demonstrated using scalable unmanned ground-aerial hybrid robots, significantly influencing M4's embedded control strategies. Research on thruster-assisted incline walking and integrated posture manipulation techniques were instrumental in refining the morphing and balancing behaviors of M4. Moreover, extensive studies on banking turns and bounding flight control provided valuable insights for integrating structural morphing with dynamic flight control strategies. [16], [31], [52]–[56]

The lab's extensive exploration into actuator fault recovery, agile flight maneuvers, and adaptive structural morphing significantly advanced the understanding necessary for M4's multi-modal transitions. Furthermore, studies on computational structure design and mechanism modeling informed mechanical optimization strategies for robustness and weight efficiency, critical for M4's new design iteration. [53], [57]–[61]

M4's implementation benefits from a deep exploration of structural and functional integrations pioneered through various lab prototypes such as Aerobat and Bat Bot, which focused on dynamic stabilization and nonholonomic constraint satisfaction. This extensive lineage of morph-

ing robots and multi-modal locomotion research positions M4 as a culmination of years of iterative innovation and systematic investigation within the lab, showcasing an advanced embodiment of bio-inspired adaptability and morpho-functional versatility. [62]

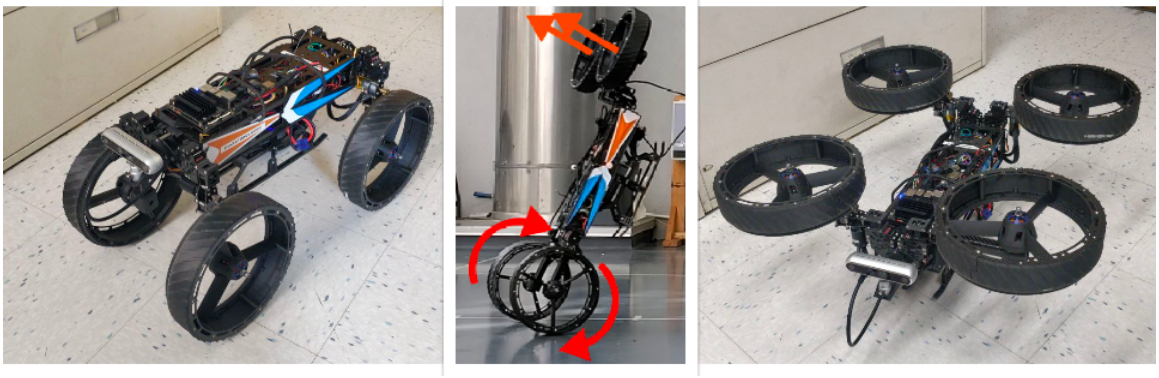

Figure 1.3: The M4 robot in various morphing configurations: rover, segway, drone [30].

1.2 Contributions and Thesis Outline

This thesis presents the mechanical design and development of **M4V0**, a significantly improved and lightweight version of the Multi-Modal Mobility Morphobot (M4). The key contributions of this work are summarized below:

Mechanical Design Contributions

- **Scaled-down architecture**: A new design was developed at **two-thirds the scale** of the previous prototype (600 mm diagonal vs. 900 mm), maintaining functionality while enabling more efficient testing.
- **Lightweight and robust**: The robot's total weight was reduced by **$\tilde{3}$9.3%** (from 5.6 kg to 3.4 kg), resulting in a **lift-to-weight ratio of 3.5:1**, and a **ground speed increase to 1.0 m/s**.
- **Cost-effective fabrication**: Unlike the previous carbon fiber and aluminum-based design, the new version uses **3D printed PLA-CF and PETG components**, making it significantly more **affordable, accessible, and modular** for rapid iteration.
- **Component optimization**: – Lightweight tire assembly reduced from 1600 g to 66.6 g – Simplified drivetrain with Dynamixel servos, reducing mechanical complexity – Reduced total

part count through the use of daisy-chained servos and one-piece assemblies – Standardized fasteners to ease maintenance and reduce tool dependency

Platform Flexibility & Prototyping

- **Modular and scalable design**: Designed to accommodate a range of microcontrollers, sensors, and actuation modules, M4V0 supports ongoing development in control strategies and locomotion research.
- **Easy part replacement**: Parts subject to wear or failure are designed for quick replacement, making M4V0 ideal for iterative testing and controller development.
- **Embedded wiring architecture**: Developed internal wire routing paths within multi-DOF joints to prevent wire damage during morphing transitions—an issue observed in previous designs.
- **Full-system prototyping**: Assembled the complete prototype in-house using **low-cost, multi-material 3D printing**, verifying structural integrity and mechanical compatibility through iterative builds.

Outline of This Thesis This report is structured as follows:

1. **Introduction and Background** – A review of the M4 platform and its bio-inspired goals
2. **Design and Methodology** – Detailed documentation of the mechanical architecture, material selection, joint design, and embedded wire routing
3. **Prototyping and Assembly Process** – An overview of the fabrication, integration, and testing methods
4. **Comparative Analysis** – Performance improvements over previous versions
5. **Conclusion and Future Work** – Reflections on system capabilities and a roadmap for autonomous multi-modal operation

Chapter 2

Literature Review

2.0.1 SOTA (State Of The Art) Designs

These examples rely on morphing of body or appendages for multi-modal transitions:

1. V. Riviere et al., 2018 [63]

   - Agile robotic fliers: A morphing-based approach
   - Multi-rotor with morphing body for aerial transitions
   - The paper presents quadrotor design with one degree of morphing freedom called Quad-Morphing Robot. With a central servo actuator, the quadrotor arms can twist about the body vertical axis to morph between two configurations: 1. Rectangular thruster placement following typical quadrotor design, 2. All four thrusters in a single line, referred to as unfolded and folded configurations, respectively. The goal of the platform is to fly through narrow gaps by reducing the wingspan of the robot through morphing. Experiments demonstrate flying through a gap of 20cmx20cm at a speed of 2.5m/s by morphing from an unfolded wingspan of 26.8cm to a folded wingspan of 12.8cm. Morphing commands were triggered based on the robot position and a cascaded PID controller tracked desired acceleration, velocity and position generated by a trajectory planner.

2. S. Ryu et al., 2020 [64]

   - Shape-morphing wheel design
   - Wheels that adapt shape for step climbing – limited aerial capability, but morphing elements.

- The paper presents a wheel mechanism that morphs into a wheg based on the rotation speed. The wheel consists of three pivoting spokes held in place by magnets such that when folded, it aligns with the circular shape of the wheel. At lower speeds, the magnetic force holds the spokes. When faced with an obstacle larger than the radius of the wheel, the robot backs up and drives the wheels at a higher speed, enabling the centrifugal force to overcome the magnets and extend the spokes. This allows the robot to climb over the obstacle following which, it returns to a normal wheel configuration by reducing its speed.

3. Michaud et al., 2003 – Azimut [22]

   - Hybrid platform with adaptive wheel-and-track.

4. Zhang et al., 2019 [65]

   - Multimodal wheel with deformable rim, allows morphing between wheel shapes.
   - The paper presents a deformable wheel design combined with a track mechanism to morph between three deformation modes: Wheel mode with a circular wheel shape, legged mode with a tall and skinny wheel shape, and track mode with a flat and wide wheel shape. By combining these deformation modes with wheel rotation and track movement, the robot can achieve locomotion on different surfaces such as fixed position track for climbing stairs, swinging tracks for fluctuating terrain, swinging legs for uneven surfaces, rolling legs for climbing obstacles.

5. L. Daler et al., 2015 [66]– Flying and walking robot

   - Robot with wings repurposed as legs, mimicking birds.
   - The paper presents a flying wing with walking capabilities by repurposing wingerons as legs for ground locomotion. In aerial mode, the wings are extended and wingerons are nominally parallel to the wings. A propeller drives the robot and the wingerons are used for control. In ground locomotion, the wing is collapsed towards the body, shortening the wingspan and the wingerons are extended as legs allowing walking.

2.0.1.1 These use separate dedicated appendages for each mode (less efficient but simpler):

1. Araki et al., 2017 [67] – Swarm of fly-drive robots

- Robots that can fly and drive, with fixed appendages for each.
- The paper presents multi-modal path planning for a swarm of "flying car" robots. The robot design is a Crazyflie drone equipped with wheels. The paper presents two planning algorithms for the swarm. Safe Interval Path Planning: extends A* to time domain by assigning "safe time intervals" to each node based on when a vehicle is passing through it. Successor Function: Finds overlapping safe intervals for all neighboring nodes to a particular state and stores node-safe interval pair as a successor state with earliest arrival time (guarantees time optimal trajectory).

2. Peterson et al., 2011 [68]

   - Wing-assisted running robot inspired by birds (WAIR style locomotion)
   - The paper presents an ornithopter design with compliant feet in a hexapod configuration. The robot, weighing 25g, uses a single actuator to drive all six legs and the wings at a frequency of 14Hz, with the legged locomotion carried out using an alternating tripod gait. This is used to perform wing assisted inclined running, demonstrating running up a 16.9 degree incline at 1.3m/s.

3. Bachmann et al., 2009 [69]

   - Biologically inspired vehicle capable of both aerial and terrestrial locomotion.
   - The paper presents the Micro Air-Land Vehicle (MALV), a 30 cm wingspan, 118 g micro-robot capable of both aerial and terrestrial locomotion via a multimodal, morphing design. Its flight system uses bat-inspired chord-wise compliant wings, enabling passive adaptive washout for gust rejection and stable low-Reynolds flight. For ground movement, it employs passively compliant wheel-legs, derived from biological principles, which allow it to crawl over obstacles taller than its own leg length (4.2 cm). MALV transitions between flight and walking and can re-launch by walking off elevated platforms. It carries a 20–25 g sensor payload and supports video transmission mid-air and on the ground.

4. Kim et al., 2021 [29]

   - A bipedal robot that can fly, slackline, and skateboard
   - Uses fixed actuators for aerial and terrestrial skills.

- The paper presents LEONARDO, a biped robot with four thrusters enabling quadrotor-like flight and thruster assisted walking. By coordinating control actions with both the legs and thrusters, it smoothly transitions between walking and flying, and performs locomotion tasks such as thruster-assisted walking on flat and slippery terrain, slackline traversal using virtual foot contact control, and dynamic balance control while riding a passive skateboard by modulating thrust-based steering and propulsion.

5. Kalantari & Spenko, 2013 – HyTAQ [70]

   - Quadrotor enclosed in a rolling cage for ground and aerial mobility.
   - The paper presents a multi-modal robot that combines a quadrotor with a freely rotating cylindrical cage to enable both aerial and terrestrial movement using the same actuators and control system. In the aerial mode, thrust from the rotors provides standard quadrotor flight control. In the terrestrial mode, the cage rolls on the ground while the quadrotor pitches to generate forward motion and heading control through thrust and thrust moments.

2.0.1.2 Combining both strategies—few known examples:

1. Baines et al., 2022 [71]

   - Adaptive morphogenesis robot
   - Repurposes flippers into legs, enables water-ground transitions.
   - The paper presents a turtle-inspired amphibious robot that employs flippers which morph into legs to enable locomotion across aquatic, terrestrial, and transitional environments. The limbs are actuated by pneumatic antagonistic pairs and composed of heat-activated variable-stiffness composites that allow reversible shape changes between flat flippers and cylindrical legs. The robot switches between swimming and walking gaits by coordinating limb geometry and control strategies. In water, it performs paddling and flapping gaits; on land, it walks with a creeping gait. On granular substrates, it adopts a belly-down crawling gait.

2. Bjelonic et al., 2020 [72]– Hybrid wheeled-legged robot

   - Uses online trajectory optimization for ground-based transitions, includes some limited morphing behaviors.

- The paper presents a quadrupedal robot with torque-controlled, non-steerable wheels on its legs that performs hybrid locomotion by combining walking and driving within the same gait cycle. The system uses an online trajectory optimization framework that splits motion planning into two parts: one for generating wheel trajectories that respect rolling constraints, and another for planning the base motion using a zero-moment point (ZMP) formulation to ensure stability. Both optimizations run in real time and are tracked by a whole-body controller.

2.0.2 Gaps

1. Limited Locomotion Plasticity in Existing Designs: Most current multi-modal robots support only two to three locomotion modes. There is a lack of systems that exhibit a wide range of versatile, plastic locomotion behaviors across diverse environments.

2. (Focus of this work) Underexplored Redundancy Manipulation through Morphing: Biological systems such as birds often repurpose appendages (e.g., wings used as legs) to adapt to different tasks, but this strategy is largely underutilized in robotics. Few designs dynamically manipulate appendage redundancy via morphing to enhance adaptability. In addition, birds combine their morphing structure and thrust vectoring to showcase multi-modal locomotion within flight envelope.

3. Scalability Challenges in Multi-Modal Platforms: Many mobile robots with soft features and shapeshifting body face issues scaling up for practical use due to added mass from mode-specific components or reliance on heavy external systems (e.g., pneumatics in soft robots). There is a need for scalable designs that remain fully functional and self-contained.

4. Inefficient Use of Mobility Components Across Modes: Existing robots often dedicate separate appendages for each mode, leading to inefficiencies in weight and complexity. There is a gap in leveraging shared, multi-functional appendages (e.g., a thruster-wheel-leg combination) to achieve compact and efficient designs.

5. Lack of Autonomous Multi-Modal Mode Switching: Although some platforms like M4 demonstrate autonomous path planning, full autonomy in switching between locomotion modes based on real-time terrain assessment and mission needs is still missing.

6. Limited Manipulation Capabilities in Mobile Morphing Robots: Object manipulation in current mobile robots is very advance. However, almost all of these methods face challenges when considered for mobile multi-modal robots. There is a gap in integrating more dexterous manipulation capabilities and structure repurposing can be an effective tool.

7. Absence of Dynamic Legged Locomotion in Morphing Systems: Legged mobility in morphing robots is often quasi-static due to mechanical limitations (e.g., high power joints). More dynamic gaits (e.g., trotting, galloping) are not yet explored in platforms that share legs with other functions like flight or rolling.

8. Insufficient Optimization of Energy-Efficient Locomotion Strategies: There is a need for better energy-aware control strategies that balance the capabilities of different modes (e.g., thruster use versus wheels) with their power demands, especially in long-duration or resource-constrained missions.

2.0.3 Proposed Solution

The focus of this work is to explore and address a critical gap in aerial robotics: the combined use of body shape morphing and thrust vectoring to achieve advanced flight capabilities that remain largely unexplored in current systems. Specifically, we aim to enable aerial platforms to dynamically recover from actuator faults and execute extremely agile maneuvers by actively translating the center of lift relative to the CoM. These capabilities are essential for enhancing fault tolerance, maneuverability, and operational versatility in complex or cluttered environments. While our proposed solutions align with the core design philosophy of the M4 platform—centered on appendage repurposing and multi-modal mobility—we significantly extend the system's capabilities by introducing new hardware design modifications. These modifications can enable in-flight morphing, allowing our robot to continuously reconfigure its structure while airborne. This contrasts with our previous work, where morphing was limited to transitions between modes on the ground or in stationary conditions. The ability to morph during flight opens the door to a richer set of control strategies, including real-time aerodynamic reconfiguration and thrust redistribution, both of which are critical for maintaining stability and performance under adverse conditions or during aggressive flight maneuvers.

Chapter 3

Hardware Design

3.1 Design Rationale

We design our robot for 4 distinct scenarios, including bridging, flattening, Segwaying, and morphing flight. We explain these scenarios.

3.1.1 Chassis Bridging

In chassis bridging mode (Fig. 3.1), the robot utilizes its adaptive structure to overcome large surface discontinuities such as ditches or trenches that would otherwise be impassable for conventional wheeled systems. As it approaches the edge of the ditch, the front wheels halt and stabilize the body. The robot then extends its chassis forward—through swinging forward its structural elements such as the appendages—to project its front end across the gap. Once the extension spans far enough, the front wheels descend and make contact with the opposite side. The robot shifts weight forward while the rear wheels provide traction, pushing the entire body over the ditch. After successful traversal, the chassis retracts back to its nominal form. This bridging approach allows the robot to maintain ground-based mobility even when terrain presents sudden voids, enabling effective deployment in unpredictable environments such as disaster zones, planetary surfaces, or rubble fields.

3.1.2 Chassis Flattening

To pass beneath low-clearance obstacles or ceiling-like barriers, the robot engages a flattening morphing mode by compressing its chassis (Fig. 3.2). Using limbs' swing motion, the robot

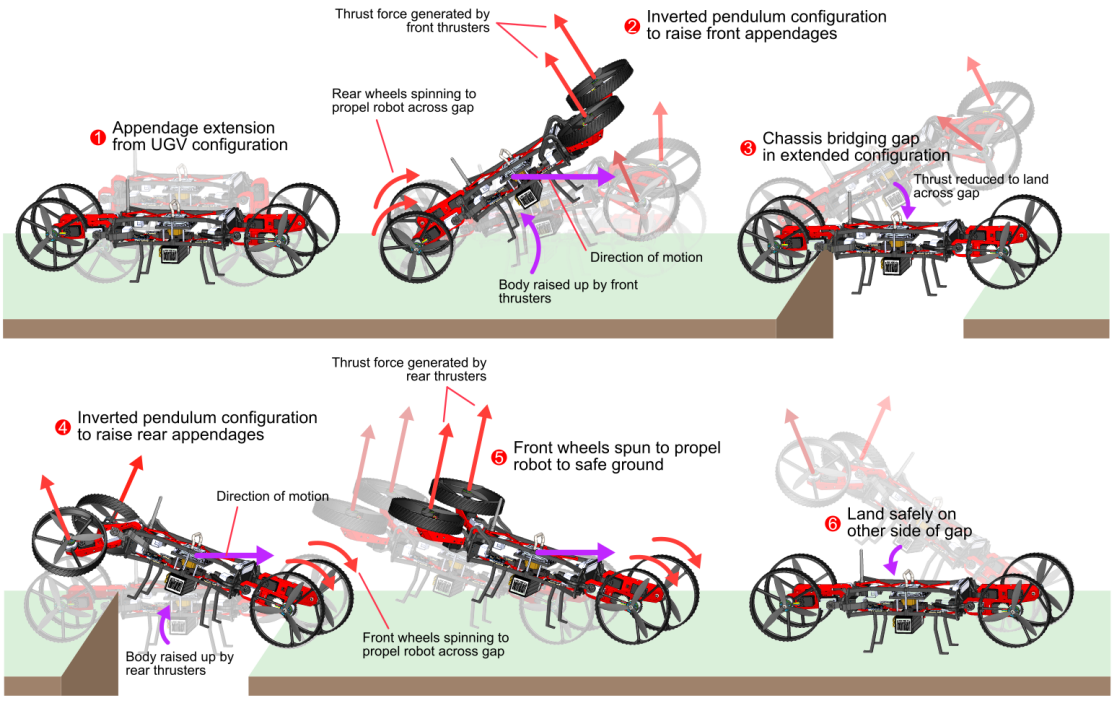

Figure 3.1: Shows a gap crossing scenario using the Chassis Bridging mode of M4. (1) The robot begins in a nominal UGV configuration, and extends its appendages to begin morphing. (2) Front appendages are lifted into an inverted pendulum pose using thrust from the front pair of propellers. (3) The robot moves forward to bridge the gap, with rear wheels spinning to generate forward motion. Thrust is modulated to control landing. (4) Rear appendages are then raised via rear thrusters. (5) Front wheels spin while thrust assists forward motion, propelling the robot over the gap. (6) The robot lands safely on the opposite side, resuming ground locomotion.

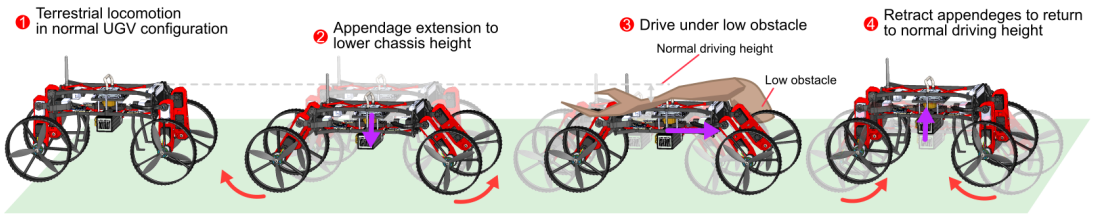

Figure 3.2: Shows chassis flattening for navigating under low-clearance obstacles. (1) The robot begins in its default UGV configuration for normal terrestrial locomotion. (2) Appendages are extended outward to actively lower the chassis height. (3) In the flattened configuration, the robot drives beneath an overhanging obstacle without contact. (4) Upon clearing the obstruction, the appendages retract to restore the original driving height.

brings its wheels closer (along body height) to the main body while folding arms and sensors outward. This reconfiguration significantly reduces its overall height, enabling it to slide or crawl under obstacles that would otherwise block passage. The robot continues moving in this low-profile configuration while maintaining adequate ground traction and orientation awareness through onboard sensors. Once the robot clears the confined space, the chassis re-extends to its original geometry, restoring full operational stance and capabilities. This capability is particularly useful in search-and-rescue scenarios, where the robot may need to pass beneath collapsed structures or debris without compromising its locomotion performance.

3.1.3 Dynamic Balancing

The dynamic balancing mode (Fig. 3.3) transforms the robot from a four-wheeled ground vehicle into a two-wheeled, self-balancing platform similar to a Segway. To initiate this transition, the robot retracts its front appendages or lifts its front limbs off the ground using jointed actuators. As the front wheels rise, the robot pivots backward and begins to balance solely on its rear wheels. A real-time control system leveraging feedback from IMUs adjusts the rear wheel torques to counteract tilting, ensuring upright stability. The robot's center of mass must be repositioned—either by internal shifting of mass or chassis tilt—to lie directly above the wheel axle for sustained balance. In this configuration, the robot achieves a narrow footprint and high maneuverability, enabling it to

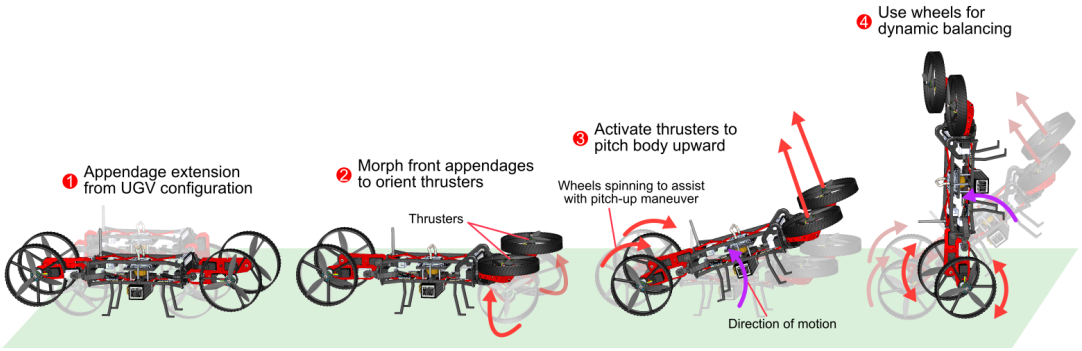

Figure 3.3: Shows M4 performing a dynamic balancing maneuver through coordinated thrust forces and wheel movements. (1) The robot begins in a nominal UGV configuration and deploys its appendages to begin morphing. (2) The front appendages are morphed to reorient thrusters for upward actuation. (3) A coordinated pitch-up motion is initiated using thrust from the front propellers and simultaneous rear wheel spin to generate angular momentum. (4) Upon achieving a vertical pose, the robot maintains balance through wheel movements

navigate slopes or prepare for further morphing, such as tumbling.

3.1.4 Morphing Flight

In morphing flight mode, the robot transitions from terrestrial locomotion to aerial mobility by reconfiguring its appendages and activating embedded thrusters. This begins with the robot adopting an upright posture—either through dynamic balancing or structural extension—followed by the outward or upward deployment of morphing limbs that house or support the thrusters. Wheels or appendages split open or rotate to expose ducted fans, which are then activated to generate lift. As the thrust gradually overcomes the weight of the robot, it lifts off the ground into free flight. During airborne operation, the robot uses thrust vectoring and closed-loop feedback from IMUs to control its orientation and trajectory in three-dimensional space. This flight mode enables rapid relocation, access to hard-to-reach locations, and hybrid mobility, combining the endurance and simplicity of wheeled motion with the agility and reach of aerial travel.

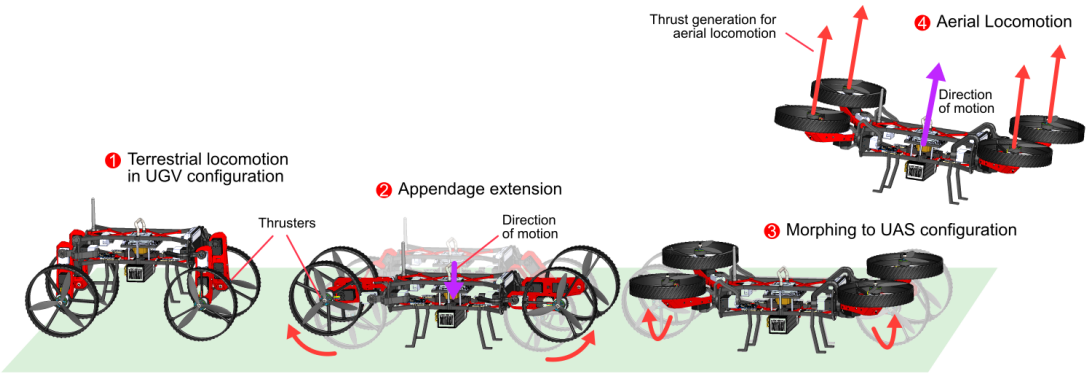

Figure 3.4: Shows the transition sequence from terrestrial to aerial locomotion for morphing flight. (1) The robot begins in a UGV configuration for terrestrial locomotion. (2) Appendages are extended outward to begin morphing transition. (3) The system morphs to a quadrotor-like configuration, reorienting the thrusters for vertical lift. (4) Thrust is generated to initiate aerial locomotion, enabling full flight capability.

3.2 Hardware Overview

In this chapter, we will describe the robot design including the body and appendage assemblies. We will present the full robot design and describe what configurations are achievable given the envisioned joints in the design. We will also cover the organization of the model including the assemblies, sub-assemblies and their locations for future developments.

3.2.1 Body Assembly

The body parts shown in Fig. 3.5 is composed of two 3D-printed frames and a pair of 3D-printed brackets. The top-left and top-right images show the top and bottom plates of the main chassis frames. These structural elements were fabricated using a Bambu Lab X1 Carbon printer, employing PLA-CF (carbon fiber reinforced polylactic acid) filament for the black segments and PETG for the red cross-members. The printing process utilized a 0.4 mm nozzle with a 0.2 mm layer height, and walls were printed with four perimeters to maximize strength under shear and bending. The infill was set to 35% in a gyroid pattern to achieve a balance between stiffness, vibration damping, and weight savings. The main frame structure consists of two longitudinal members with embedded cross-bracing in a scissor or X-pattern (colored red), designed to enhance torsional stiffness and distribute loads uniformly while minimizing overall mass. The red members are printed

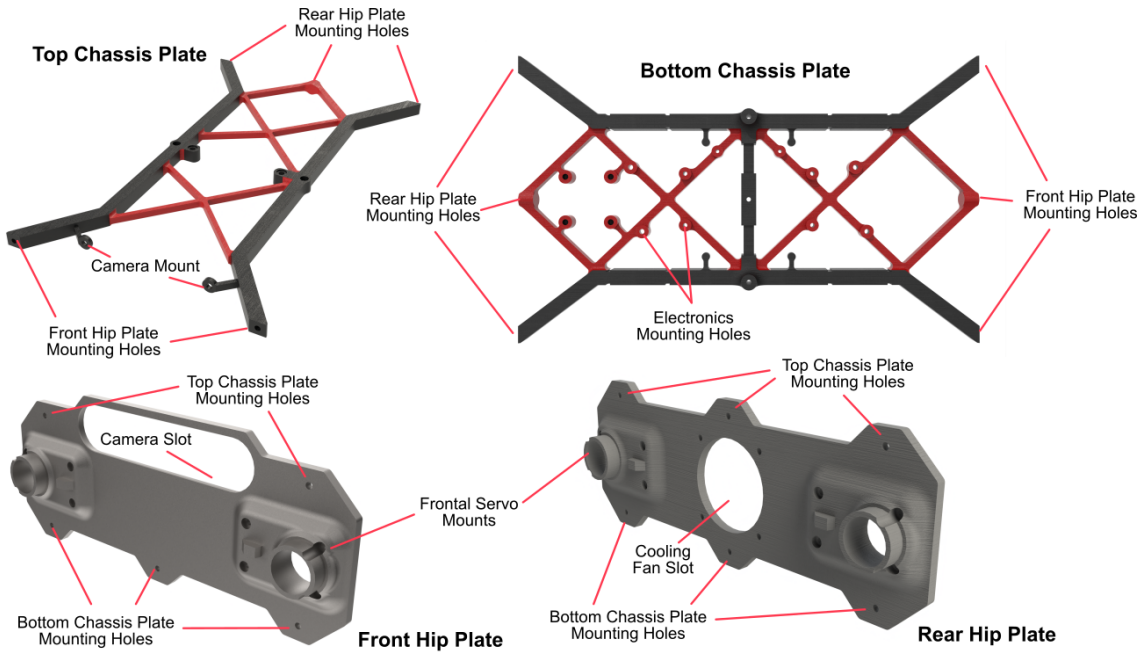

Figure 3.5: Primary structural components of the robot chassis, highlighting mounting interfaces for electronics, sensors, and appendages across the top plate, bottom plate, and front/rear hip plates.

as detachable inserts to allow color/material variation and easy replacement. The angled view (top-left) reveals mounting features and cutouts for integrating actuators, sensors, or pivot joints for foldable or transformable configurations. The top-down view (top-right) further clarifies the symmetric layout, with mounting holes and integrated alignment slots that accommodate modular payloads or drivetrain sub-assemblies.

In Fig. 3.5, the bottom images display the two 3D-printed brackets that serve as interface modules between the frame and locomotion components such as wheels or actuators. The left bracket is also fabricated using PLA-CF with 100% infill around critical load-bearing zones — particularly near the cylindrical bosses used for bearing press-fits and motor shaft clearance. The front and rear brackets share the same general geometry, but the rear version (right image) was designed with simplified mechanical features to streamline the printing process and reduce material usage, trading off some precision and stiffness for faster prototyping. Both brackets include alignment bosses, axle ports, and mounting holes that interface seamlessly with the frames. Their consistent geometry ensures interchangeability and supports a modular design philosophy, enabling quick swaps or reconfigurations of drivetrain assemblies without redesigning core chassis components.

The chassis of the robot encloses all onboard processing and power electronics. Flight

actuation in UAS mode is managed by a Pixhawk Orange Cube Plus Flight Controller Unit (FCU), mounted to the lower chassis plate. Mounted above the FCU using nylon standoffs is an Nvidia Jetson Orin Nano module, which handles higher-level autonomy tasks as well as wheel and joint actuation. Joint actuation is performed by DYNAMIXEL XM430-W210-T servos. These are connected via communication lines arranged in a star topology: each leg of the robot contains a daisy-chained group of three servos, and each of these chains radiates from a central hub, forming the star configuration. Communication is facilitated through a U2D2 module that connects to the Jetson Orin Nano via USB, serving as a UART-to-TTL bridge. The robot is powered by a 6s 5200 mAh 50C Lithium Polymer battery mounted beneath the chassis with Velcro straps for convenient access and replacement. Power is routed through a distribution board mounted to the bottom chassis plate, supplying 12V to the Jetson Orin Nano and joint servos, 5V to the FCU, and a nominal 22V to the flight motors.

Filament	**Impact Strength (XY) [kJ/m^2]**	**Bending Strength (XY) [MPa]**	**Bending Modulus (XY) [MPa]**	**Impact Strength (Z) [kJ/m^2]**	**Heat Deflection Temp. (0.45 MPa) [°C]**	**Water Absorption (25°C, 55% RH) [%]**
PLA	26.6	76.0	2750.0	13.8	57.0	0.43
PETG	52.7	65.0	1670.0	13.6	69.0	0.32
ABS	39.3	62.0	1880.0	7.4	87.0	0.65
ASA	41.0	65.0	1920.0	4.9	100.0	0.45
PC	34.8	108.0	2310.0	9.0	117.0	0.25
TPU 95A	125.2	20.0	295.0	88.7	70.0	1.16
PLA-CF	23.2	89.0	3950.0	7.8	55.0	0.42
PETG-CF	41.2	70.0	2910.0	10.7	74.0	0.33
PA6-CF	40.3	151.0	5460.0	15.5	184.0	2.35
PAHT-CF	57.5	125.0	4230.0	13.3	140.0	0.84
PET-CF	36.0	131.0	5320.0	4.5	205.0	0.37
PPA-CF	41.7	142.0	7160.0	4.3	227.0	1.30
PPS-CF	27.8	208.0	9860.0	2.8	264.0	0.05

Table 3.1: Mechanical and thermal properties of various 3D printing filaments. [73]

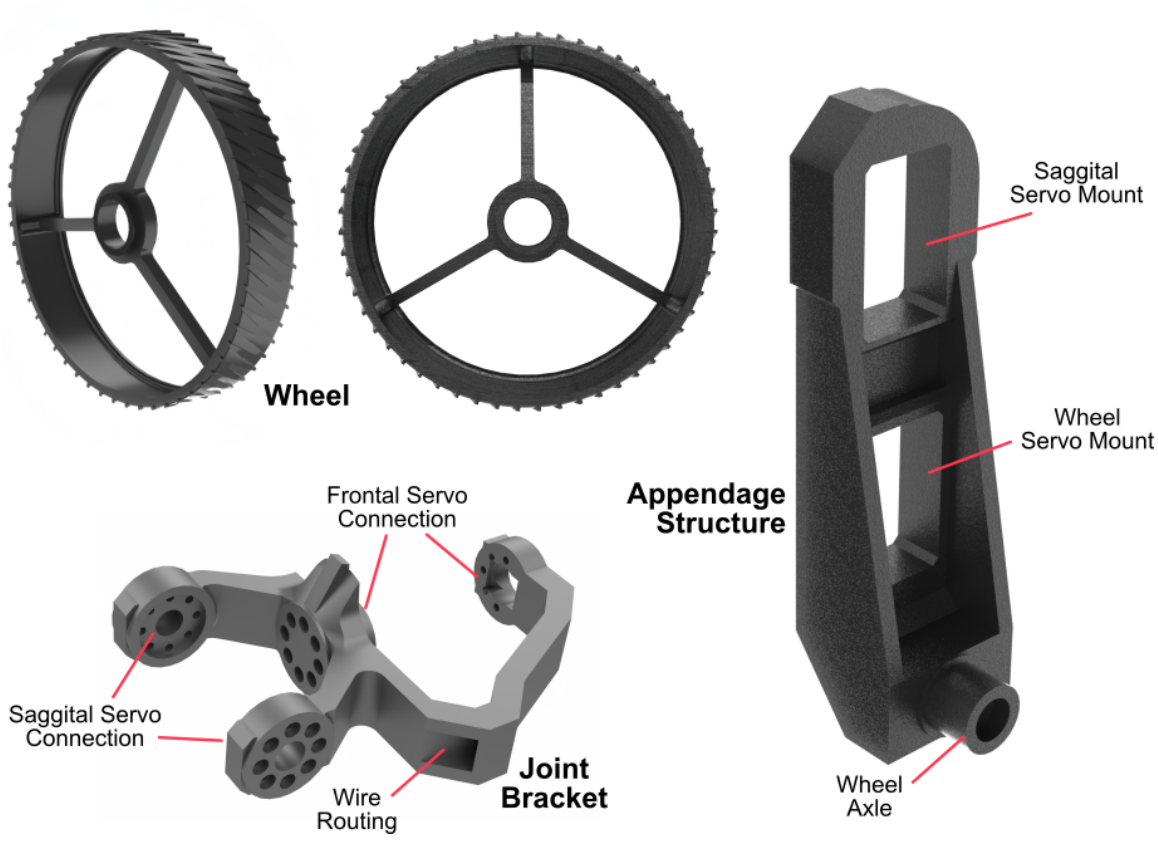

Figure 3.6: Key mechanical components of the robot's appendage, including the wheel, joint bracket, and appendage structure.

3.2.2 Appendage Assembly

In Fig. 3.6, the top part is a drive wheel featuring a high sidewall and internal spokes designed for structural efficiency. The angled perspective reveals a circular profile with a grooved tread optimized for wheeled or tracked locomotion. The outer surface includes a ribbed or toothed pattern to enhance traction on slippery or uneven terrain. Internally, the wheel uses a thin three-spoke layout to support the central hub, effectively reducing weight while maintaining radial symmetry and structural integrity. This component is 3D-printed using PETG or PLA-CF on a Bambu Lab printer with moderate infill (typically 25–40%) in a gyroid or cubic pattern. Due to its relatively flat geometry, the part can be printed with minimal support material, facilitating faster and more efficient fabrication. The adjacent appendage design is a vertically oriented, load-bearing structural element, likely serving as a leg or suspension arm. It includes elongated rectangular cutouts along the body, which reduce weight and provide space for cable routing or embedded sensors. The bot-

tom cylindrical boss acts as a pivot axis and bushing interface, anchoring the wheel assembly and allowing rotational motion. The upper arched region interfaces with the robot's main chassis or subframe. The overall geometry—with its tall profile, hollowed sections, and ribbed contours—is engineered to withstand significant bending loads and vertical forces encountered during locomotion or appendage articulation. The component shown at the bottom left is a multi-degree-of-freedom hub or joint interface, functioning as a central coupling unit for the appendage and hip actuator. It includes several circular flanges, each with symmetrically distributed mounting holes, designed for direct integration with actuators or transmission mechanisms. The core "spine" links these radial branches and serves as the primary structural connection between the limb and the robot's torso. The design demonstrates smooth filleting and geometric transitions between limbs to preserve material continuity, distribute stresses evenly, and prevent mechanical failure under dynamic loading conditions.

Assembly begins with mounting the flanged ultra-thin ball bearings connecting the axel on the leg to the wheel well. The wheel is then seated, and a matching flanged bearing is inserted on the outer side connecting the wheel and a BLDC motor mount. An M4 spindle bolt (50 mm, M4×0.70 mm thread) and a serrated M4 spindle nut clamp the axis in firmly place. Motor wires for the T-motor V2812 BLDC are then routed through internal cable channels located beneath the bearing seats and along the inner walls of the leg, following which, the BLDC flight motor is secured to its mounting plate. The propeller (7.5-inch tri-blade, T-Motor C7.5x4.6x3) is mounted onto the motor shaft and secured with an M5 prop lock nut. Following this, the Dynamixel XM430-W210-T servo responsible for driving the wheel is inserted into its socket and bolted from both sides with M2x10 bolts. Finally, a second Dynamixel servo is installed on the top interface of the leg, after which the hip joint is mounted and bolted, completing the appendage assembly.

3.3 Full CAD Model

This section presents:

1. Detailed location of the CAD model folder and access information.
2. Comprehensive list of all components.
3. Breakdown of all component weights (CAD estimations and experimental measurements).
4. Detailed list of subassemblies.

S.No	Component Name	Description	Weight (g)	Qty	Total Weight (g)
1	7.5_inch_prop	7.5_inch_(representation)_3 blade propeller melhorado	4.96	4	19.84
2	M2.5x12Lg_SHSC	Pixhawk screw	0.6209	4	2.4836
3	M3x4_4Lg_Heat-inserts	PDB mount	0.252593	4	1.010372128
4	M3x5Lg_Plastic_SHSC	PDB mount	0.0761	4	0.3044
5	M2x10Lg_SHSC	U2D2 screws	0.3439	2	0.6878
6	M3x52Lg_Nylon-standoff_Female	Mounting top & base frame	1.77	2	3.54
7	M2.5x37Lg_hex-standoff	Jetson mount	0.7	4	2.8
8	M4x6Lg_SHSC	Realsense mount	1.5	2	3
9	Special-screws_M3x10Lg_ Flanged-Button-Head-Screws	Frame front and back mount	0.734	11	8.074
10	M2.5x14Lg_SHSC	Hip servos (4)	0.68	16	10.888
11	M2x22Lg_SHSC	Hip servo output shaft mounting screws	0.5713	32	18.2816
12	M2x8Lg_SHSC	Leg assembly (knee) servo output screws	0.3069	128	39.2832
13	M2.5x12Lg_SHSC	Leg assembly (knee) servo mount screws set 1	0.6209	8	4.9672
14	M2.5x10Lg_SHSC	Leg assembly (knee) servo mount screws set 2	0.5616	8	4.4928
15	M4x50Lg_spindle-bolt_Hex-head	Spindle bolt	5.5008	4	22.0032
16	M4_Spindle_nut	Spindle nut serrated flanged	1.3859	4	5.5436
17	20x27x4_Flanged Ultra-Thin Ball Bearing	Hub bearings - wheel	5.940604	8	47.52483024
18	M5_prop-lock-nut	Motor prop nuts – comes with motor	1.915	4	7.65
19	M3x8Lg_SHSC	BLDC mounting bolts – comes with motor	0.81	16	12.96
20	M3x25_SHSC	Cooling fan mounting - partially threaded	1.65	4	6.6104
21	M3_flanged-serrated-nut	Cooling fan mounting nut serrated	0.76	2	1.52
22	Special-screws_8–32 Thread Size, 7–16inch	Handle mounting screws	1.8518	2	3.7036
23	Handle	Support for top frame	17.00	1	17.8671
24	Battery strap 20x500	Velcro strap for mounting battery	2	2	4
25	Nylon Plastic Cable Tie	For mounting ESCs	0.50	8	4
26	Nvidia_Jetson_Orin_Nano	Nvidia Jetson Orin Nano Developer kit	176.00	1	176
27	DYNAMIXEL XM430-W210-T	Servo with cable - all joints	84.20	12	1010.4
28	V2812 t-motor	Flight motor	78.00	4	312
29	Low-Voltage Equipment-Cooling Fan	Cooling fan for the bot	12.44	1	12.4386
30	PDB	Power distribution board	21.00	1	21
31	U2D2	Controlling dynamixels	9.00	1	9
32	Telemetry_module	Telemetry module	14.00	1	14
33	RC_receiver	Receiver	16.00	1	16
34	Realsense	D455	103.00	1	103
35	Flight_controller	Pixhawk cube orange	75.00	1	75
36	Teensy_4.1	Teensy 4.1	8.00	1	8
37	Battery	5000mAh 6S Lipo Battery EC5 50C-100C	725.00	1	725

Table 3.2: Bill of Materials with Descriptions and Weights

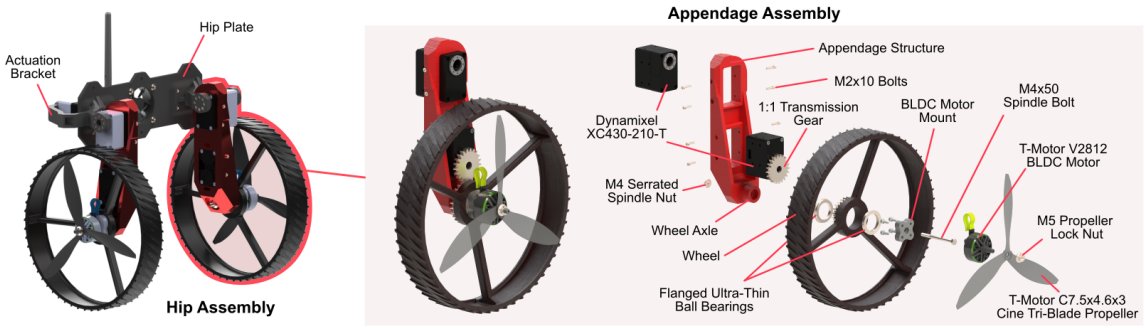

Figure 3.7: Detailed view of the robot appendage, including hip assembly (left) and exploded appendage assembly (right). The hip assembly integrates a dual-servo actuation mechanism mounted to the hip plate. The appendage assembly features a Dynamixel XC430-210-T servo coupled to a 1:1 transmission gear, enabling rotation of the wheel about the appendage axis. A BLDC motor (T-Motor V2812) mounted inside the wheel hub drives a tri-blade propeller (T-Motor C7.5x4.6x3) for aerial locomotion. Structural components include the appendage frame, joint bracket, and flanged ultra-thin ball bearings for low-friction wheel rotation. All parts interface using standard fasteners and spindle bolts for ease of assembly and maintenance.

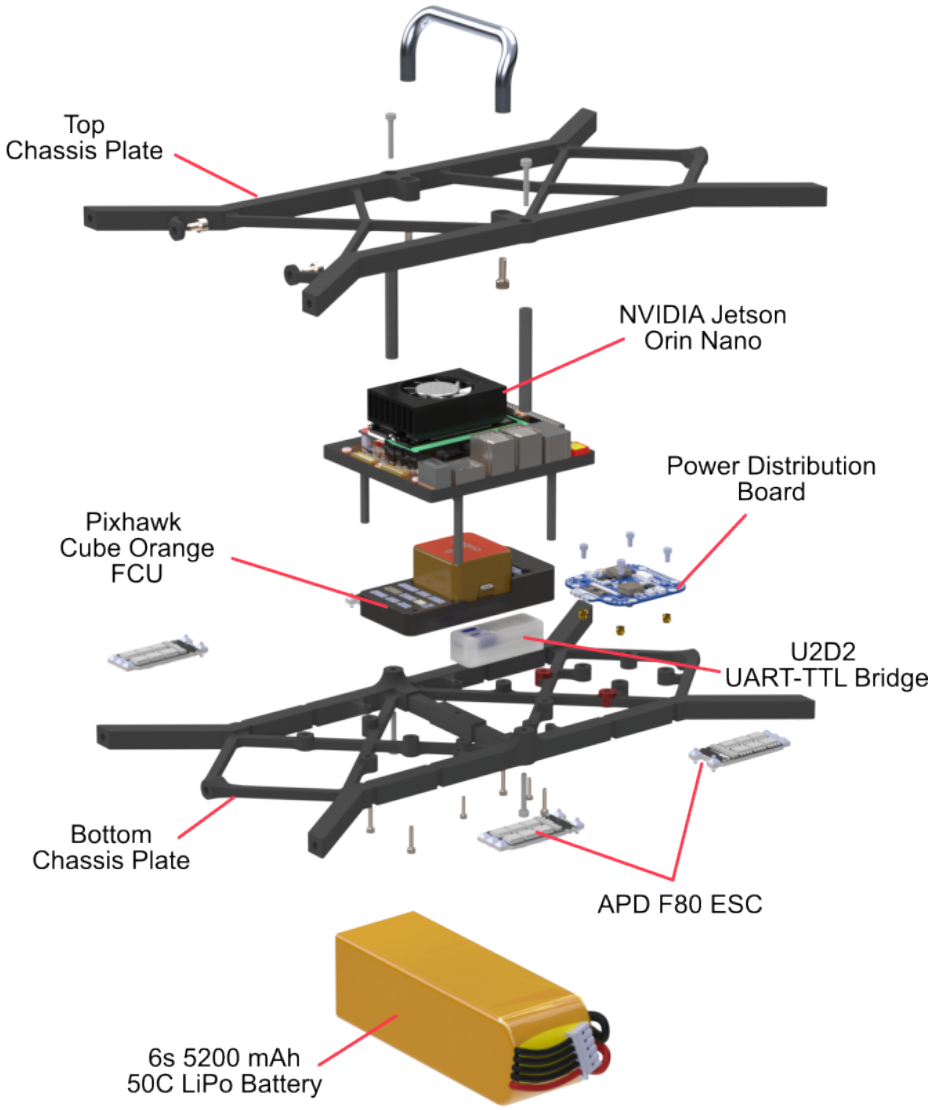

Figure 3.8: Exploded view of the onboard electronics stack within the main chassis. The system integrates a Pixhawk Cube Orange flight controller for low-level control, an NVIDIA Jetson Orin Nano for onboard compute, and a power distribution board to manage supply lines. These are housed between the top and bottom chassis plates with standoff mounts. An APD F80 electronic speed controller (ESC) drives the propulsion system, and a U2D2 UART–TTL bridge provides communication with joint actuators. Power is supplied by a 6s 5200 mAh 50C LiPo battery mounted beneath the lower chassis plate.

Chapter 4

Testing and Results

This chapter provides a brief overview of the validation process for the M4-v0 robot, including details of the prototype fabrication, experimental testing procedures, observed performance metrics, and qualitative evaluations of its multimodal transitions. The goal of this testing phase was to evaluate the robot's ability to reliably perform terrestrial and aerial locomotion while successfully executing structural morphing behaviors such as chassis bridging, chassis flattening, dynamic balancing, and full morphing flight.

4.1 Prototype Overview and Scale Considerations

The prototype constructed for this testing phase represents a 2/3 scale model of the original M4 system. This scaling was necessary due to material constraints, manufacturing time limitations, and to facilitate faster iteration cycles during prototyping. Despite its reduced dimensions, the prototype preserves all core mechanical features, embedded actuation systems, and sensor integration found in the full-scale design. A key aspect of the prototype was attaining a **2:1 thrust-to-weight ratio**. Simultaneously, the TTOW was approximately half of the full design's expected load, which ensured safe testing and simplified failure recovery procedures during early trials.

4.2 Tests

Mode transition experiments was conducted to validate the robot's ability to execute all four major morphing behaviors. These experiments were conducted in indoor lab environments.

For each experiment, video documentation, telemetry logging, and manual observations were used to assess reliability, repeatability, and actuation fidelity.

Initial ground locomotion focused on validating the robot's performance in its nominal ground wheeled configuration. The robot was tested to navigate a flat indoor surface, demonstrating traction, turning radius, and system responsiveness.

Chassis bridging was envisioned as a morphing maneuver to enable the robot to overcome large surface discontinuities, such as trenches or terrain voids, which are typically impassable for conventional ground robots. In this mode, the robot would approach a gap and initiate appendage reconfiguration, lifting the front limbs into an inverted pendulum pose to project the front wheels across the void. Once the front wheels made contact with the opposite edge, coordinated thrust would assist in forward pitching, enabling the rear section of the robot to traverse the gap. The concept integrates both propeller-based lift and ground wheel propulsion to execute the crossing maneuver in a dynamically stable manner. This bridging behavior, although not experimentally evaluated in this prototype cycle, remains a central use-case scenario for validating M4's multimodal mobility capabilities in future testing campaigns.

To test chassis flattening, a horizontal obstacle with a clearance of 12 cm was positioned along the robot's planned path. The robot successfully transitioned into a flattened profile by rotating its limbs outward and lowering its chassis height. It then navigated under the obstacle without any collisions. The appendages were then retracted and the robot resumed normal height. This scenario simulated collapsed ceilings and cluttered search-and-rescue environments where such a mode would be mission-critical.

4.3 Integration Achievements and Challenges

Throughout the integration process, several critical milestones were reached. First, a functional wire-routing strategy was implemented to preserve cable integrity through 2-DoF joints. This ensured electrical continuity to motors and sensors even during complex morphing transitions. Second, onboard compute (Jetson Orin Nano) and power distribution components were tested for thermal reliability, confirming the platform's potential for closed-loop autonomy.

Challenges observed included:

- **Thermal dissipation**: The enclosed electronics experienced occasional heat buildup under extended operation.

- **Vibration management**: At high throttle, the propeller-induced vibrations propagated through 3D-printed structures, slightly impacting sensor accuracy.
- **Joint compliance**: Due to the polymeric hinge materials, some backlash was noted during high-load transitions. Future designs may include embedded damping or reinforced joints.

In summary, this chapter validates the functional capabilities of the M4 robot in real-world environments. The 2/3 scale prototype successfully demonstrated all four key locomotion modes, including complex morphing transitions between terrestrial and aerial states. The results confirm the feasibility of a fully embedded, structurally morphing robotic platform for hybrid mobility in unstructured or extreme environments. These findings form a foundation for future enhancements in autonomous planning, structural refinement, and long-term field deployment.

Figure: 4.1 illustrates the transformative capability of the M4 prototype transitioning from a ground-based wheeled configuration into an aerial flight configuration. This morphing is facilitated by dynamically reorienting its appendages into a quadrotor-like layout. The innovative feature here is the integration of thrusters directly within the wheel assemblies, allowing each limb to seamlessly transition from a terrestrial locomotion component into an aerial propulsion unit. This embedded morphing ability significantly improves the operational versatility of the robot, enabling it to rapidly overcome terrestrial obstacles through vertical lift and aerial mobility. The configuration allows the M4 prototype to access challenging or obstructed areas that traditional ground robots cannot navigate, considerably broadening its application scope.

Figure: 4.2 demonstrates the chassis flattening maneuver, where the robot actively reduces its vertical profile to pass beneath low-clearance obstacles. The innovative mechanical feature employed here involves strategic rotation and extension of appendages outward, thus significantly reducing the chassis height without compromising its stability or mobility. This maneuver enhances the robot's capability to operate in constrained environments, making it particularly advantageous for search-and-rescue scenarios or exploration in collapsed structures. The robot's ability to revert quickly and reliably to its original form after clearing obstacles illustrates robust mechanical integration and reliable repeatability, essential for field operations.

Figure: 4.3 highlights the robot's ability to transition directly from a crawling configuration, optimized for stable and controlled ground movements over uneven terrain, into a flight configuration optimized for vertical and horizontal aerial mobility. This rapid morphing capability leverages multi-degree-of-freedom appendages and integrated actuators, significantly reducing transition times between locomotion modes. This seamless integration allows the robot to dynami-

cally adapt to terrain changes without external intervention, significantly increasing its autonomous operational potential and enhancing mission efficiency, especially in dynamic and unpredictable environments.

Figure: 4.4 illustrates an **alternative, diagonally-phased morphing sequence** from crawling to flight configuration. Unlike the front-pair-first approach in Figure 4.3, this maneuver begins with the two opposing diagonal limbs while the remaining pair maintains ground contact. This staggered deployment offers four advantages:

1. **Enhanced static stability** – a three-point support polygon is preserved longer, preventing tip-over even on uneven terrain.

2. **Lower peak power demand** – dividing the actuation into two phases halves the instantaneous current draw, easing stress on the battery and ESCs.

3. **Mid-sequence fail-safe** – if a fault is detected after phase 1, the robot can abort and revert to crawling without committing to flight, boosting operational robustness.

4. **Gentler center-of-mass migration** – incremental appendage reorientation minimizes sudden COM shifts, reducing corrective torque requirements on wheel servos.

Together, these benefits demonstrate the controller's flexibility to select morphing trajectories that trade speed for energy efficiency and risk mitigation, broadening the robot's mission-specific adaptability.

Figure: 4.5 showcases the approach of embedded wire routing within the appendage structures of the M4 prototype. The internal routing channels securely house wiring, protecting critical electrical connections during complex movements and transformations. This feature addresses a common issue in robotic appendages—wire damage from repeated articulation. By embedding wiring within structural components, the risk of cable wear or interference during morphing and locomotion transitions is greatly mitigated, enhancing the robot's overall reliability, operational longevity, and maintenance convenience. This improvement directly translates into fewer field failures and lower operational downtime, vital for prolonged deployment in harsh environments.

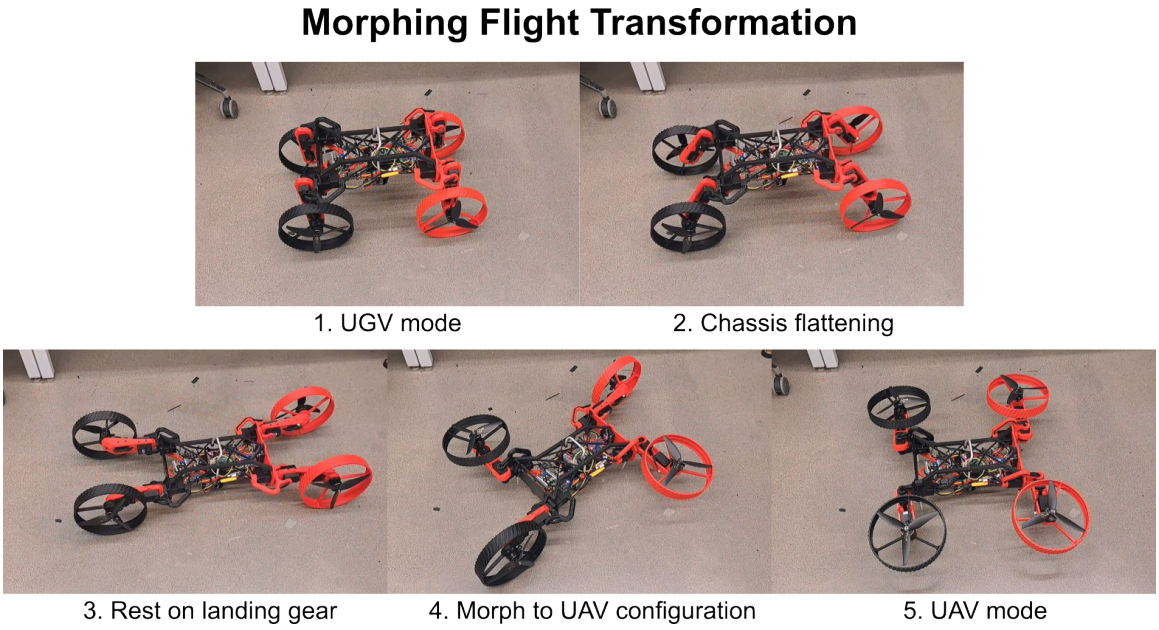

Figure 4.1: Shows the new M4 prototype transforming configurations for morphing flight.

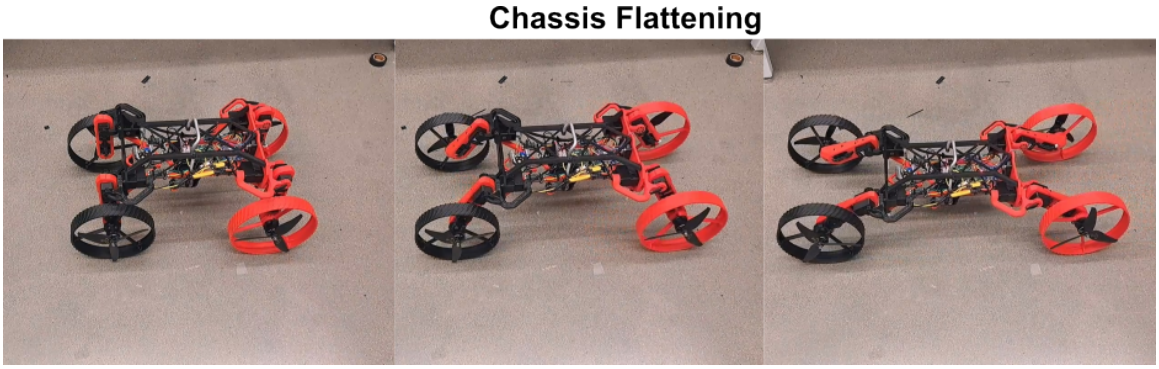

Figure 4.2: Shows M4 prototype executing Chassis Flattening maneuver.

Figure 4.3: Shows M4 prototype executing morphing from crawling configuration to flight configuration.

Figure 4.4: Shows M4 prototype executing a different sequence of morphing from crawling configuration to flight configuration.

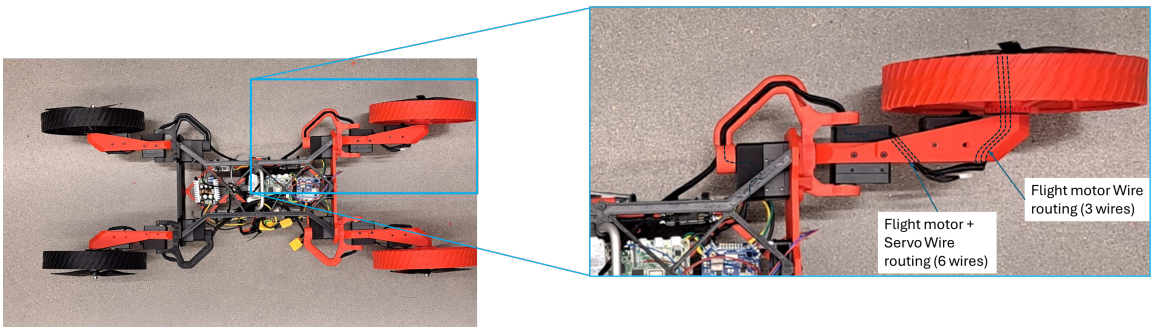

Figure 4.5: Shows embedded wire routing through the appendages.

Chapter 5

Conclusion

This thesis presented the complete design, fabrication, and conceptual validation of the M4-v0, a structurally morphing robotic platform capable of transitioning between wheeled, legged-like, and aerial locomotion modes. The design philosophy of M4 was centered on the principles of appendage repurposing and structural integration—leveraging shared mechanical and actuation components to support radically different locomotion strategies. This work contributes to a growing body of research focused on developing robots capable of navigating unstructured, extreme environments where conventional single-mode systems fail.

The first set of contributions lies in the hardware realization of the M4 platform. We achieved a fully embedded, 2/3-scale prototype constructed using high-strength 3D-printed polymer composites and off-the-shelf actuators. The mechanical architecture was carefully engineered to support the structural loads associated with aerial lift, while maintaining the compliance and mechanical accessibility required for wheeled and dynamic balancing operations. A fully integrated electronics stack was implemented, comprising an onboard compute module (NVIDIA Jetson Orin Nano), flight controller (Pixhawk Cube Orange), joint control via Dynamixel servos, and a custom power distribution board. Special attention was given to wire routing and packaging across multiple degrees of freedom to preserve cable continuity during morphing transitions.

Through conceptual testing and operational demonstrations, the prototype validated key aspects of M4's design intent. Ground locomotion in wheeled configuration showed acceptable performance. While the robot did not transition between different configurations, such as dynamic balancing (Segway-like operation), chassis flattening for low-clearance traversal, and aerial morphing for vertical takeoff, the feasibility was inspected by manually positioning the arms. The aerial mode inpsections based on body weight and spec sheet data from motor manufacturer shows suffi-

cient thrust-to-weight ratio (approximately 2:1) to achieve lift and short-duration hover.

Several open questions remain that will guide the next stages of development. First, full autonomy in mode selection and terrain-aware reconfiguration remains an open challenge. The ability for M4 to autonomously sense, classify, and respond to terrain variations by switching between locomotion modes is critical for long-duration deployment in unknown environments. Future work must focus on integrating perception modules (e.g., depth sensing, terrain segmentation), adaptive decision-making policies, and reinforcement learning or behavior trees for high-level control.

Second, the long-term mechanical durability of appendages under repeated morphing transitions and high-thrust operations remains unquantified. Future work should investigate fatigue resistance, impact resilience, and structural integrity through extended durability testing. Embedding passive compliance or damping in key joints may help mitigate vibrations and extend operational life.

Third, thermal management in enclosed embedded systems poses a practical concern, particularly under continuous or compute-intensive operation. Future iterations should explore heat sinks, forced air cooling, and thermal-aware power distribution strategies to maintain onboard electronics within safe operating ranges.

Fourth, energy-efficient trajectory planning for morphing systems is another underexplored domain. While the current system relies on manual or scripted transitions, future work should incorporate model predictive control (MPC), energy-aware planners, or contact-implicit optimization methods to balance the cost of mode switching with mission goals.

Finally, a broader set of environments—such as rugged outdoor terrain, collapsed infrastructure, or Martian analog sites—must be explored to comprehensively evaluate the M4 platform's real-world applicability. Field trials, long-range autonomy experiments, and cooperative tasks involving multi-agent coordination are all compelling extensions of this work.

In summary, the M4-v0 robot establishes a strong foundation for the future of structurally morphing, multi-modal mobile systems. By advancing mechanical design, integration, and concept-level validation, this work contributes toward the development of agile, adaptable robotic platforms suited for search-and-rescue, exploration, and inspection missions in the most demanding operational environments.

Bibliography

[1] E. Sihite, A. Kalantari, R. Nemovi, A. Ramezani, and M. Gharib, "Multi-modal mobility morphobot (m4) with appendage repurposing for locomotion plasticity enhancement," *Nature communications*, vol. 14, no. 1, p. 3323, 2023.

[2] A. Ramezani and K. Sreenath, "Thruster-assisted legged mobility for explorations on mars," *LPI Contributions*, vol. 2655, p. 5074, 2022.

[3] E. Sihite, P. Dangol, and A. Ramezani, "Unilateral ground contact force regulations in thruster-assisted legged locomotion," in *2021 IEEE/ASME International Conference on Advanced Intelligent Mechatronics (AIM)*, IEEE, 2021, pp. 389–395.

[4] P. Dangol, E. Sihite, and A. Ramezani, "Control of thruster-assisted, bipedal legged locomotion of the harpy robot," *Frontiers in Robotics and AI*, vol. 8, p. 770 514, 2021.

[5] P. Dangol and A. Ramezani, "Reduced-order-model-based feedback design for thruster-assisted legged locomotion," *arXiv preprint arXiv:2105.10082*, 2021.

[6] P. Dangol, A. Ramezani, and N. Jalili, "Performance satisfaction in midget, a thruster-assisted bipedal robot," in *2020 American Control Conference (ACC)*, IEEE, 2020, pp. 3217–3223.

[7] P. Dangol, A. Lessieur, E. Sihite, and A. Ramezani, "A hzd-based framework for the real-time, optimization-free enforcement of gait feasibility constraints," in *2020 IEEE-RAS 20th International Conference on Humanoid Robots (Humanoids)*, IEEE, 2021, pp. 156–162.

[8] P. Dangol, A. Ramezani, and N. Jalili, "Performance satisfaction in harpy, a thruster-assisted bipedal robot," *arXiv preprint arXiv:2004.14337*, 2020.

[9] P. Dangol and A. Ramezani, "Thruster-assisted legged robot control (conference presentation)," *Unmanned Systems Technology XXII*, vol. 11425, p. 1 142 507, 2020.

[10] A. C. de Oliveira and A. Ramezani, "Thruster-assisted center manifold shaping in bipedal legged locomotion," in *2020 IEEE/ASME International Conference on Advanced Intelligent Mechatronics (AIM)*, IEEE, 2020, pp. 508–513.

[11] P. Dangol and A. Ramezani, "Feedback design for harpy: A test bed to inspect thruster-assisted legged locomotion," in *Unmanned Systems Technology XXII*, SPIE, vol. 11425, 2020, pp. 49–55.

[12] A. Salagame, S. Manjikian, C. Wang, *et al.*, "A letter on progress made on husky carbon: A legged-aerial, multi-modal platform," *arXiv preprint arXiv:2207.12254*, 2022.

[13] P. Dangol and A. Ramezani, "Towards thruster-assisted bipedal locomotion for enhanced efficiency and robustness," *IFACPapersOnLine*, vol. 53, no. 2, p. 10 019, 2020.

[14] A. Ramezani, *Morpho-functional robots with legged and aerial modes of locomotion*, US Patent App. 17/777,743, Jan. 2023.

[15] C. Wang, *Leggedwalking on inclined surfaces*, 2023. arXiv: 2306.00179 [cs.RO].

[16] E. Sihite, F. Slezak, I. Mandralis, *et al.*, "Demonstrating autonomous 3d path planning on a novel scalable ugv-uav morphing robot," *arXiv preprint arXiv:2308.00235*, 2023.

[17] A. Ramezani and M. Gharib, *Multi-modal mobility unmanned vehicle*, US Patent App. 18/055,757, May 2023.

[18] A. Ramezani, E. Sihite, S. Devey, and M. Gharib, "Efficient and endured aerial mobility on mars using novel morphing micro aerial vehicle designs," *LPI Contributions*, vol. 2655, p. 5051, 2022.

[19] B. Mottis, "Epfl master thesis: Efficient path planning of m4, mars multi-modal morphofunctional rover," 2022.

[20] A. Kalantari and M. Spenko, "Modeling and performance assessment of the hytaq, a hybrid terrestrial/aerial quadrotor," *IEEE Transactions on Robotics*, vol. 30, no. 5, pp. 1278–1285, 2014.

[21] A. Kossett, R. D'Sa, J. Purvey, and N. Papanikolopoulos, "Design of an improved land/air miniature robot," in *2010 IEEE International Conference on Robotics and Automation*, 2010, pp. 632–637.

[22] F. Michaud, D. Létourneau, M. Arsenault, *et al.*, "Multi-modal locomotion robotic platform using leg-track-wheel articulations," *Auton. Robots*, vol. 18, pp. 137–156, Mar. 2005.

[23] L. Cui, P. Cheong, R. Adams, and T. Johnson, "AmBot: A Bio-Inspired Amphibious Robot for Monitoring the Swan-Canning Estuary System," *Journal of Mechanical Design*, vol. 136, no. 11, Oct. 2014.

[24] Y. de Viragh, M. Bjelonic, C. D. Bellicoso, F. Jenelten, and M. Hutter, "Trajectory optimization for wheeled-legged quadrupedal robots using linearized zmp constraints," *IEEE Robotics and Automation Letters*, vol. 4, no. 2, pp. 1633–1640, 2019.

[25] A. J. Ijspeert, A. Crespi, D. Ryczko, and J.-M. Cabelguen, "From swimming to walking with a salamander robot driven by a spinal cord model," *Science*, vol. 315, no. 5817, pp. 1416–1420, 2007.

[26] E. Sihite, B. Mottis, P. Ghanem, A. Ramezani, and M. Gharib, "Efficient path planning and tracking for multi-modal legged-aerial locomotion using integrated probabilistic road maps (prm) and reference governors (rg)," in *2022 IEEE 61st Conference on Decision and Control (CDC)*, 2022, pp. 764–770.

[27] Y. Mulgaonkar, B. Araki, J.-s. Koh, *et al.*, "The flying monkey: A mesoscale robot that can run, fly, and grasp," in *2016 IEEE International Conference on Robotics and Automation (ICRA)*, 2016, pp. 4672–4679.

[28] N. Meiri and D. Zarrouk, "Flying star, a hybrid crawling and flying sprawl tuned robot," in *2019 International Conference on Robotics and Automation (ICRA)*, 2019, pp. 5302–5308.

[29] K. Kim, P. Spieler, E.-S. Lupu, A. Ramezani, and S.-J. Chung, "A bipedal walking robot that can fly, slackline, and skateboard," *Science Robotics*, vol. 6, no. 59, eabf8136, 2021.

[30] F. Slezak, "A first step towards autonomous multi-modal navigation onboard the m4 robot - hybrid ugv/uav," 2022.

[31] E. Sihite, A. Salagame, P. Ghanem, and A. Ramezani, "Actuation and Flight Control of High-DOF Dynamic Morphing Wing Flight by Shifting Structure Response," in *2023 62nd IEEE Conference on Decision and Control (CDC)*, Dec. 2023, pp. 8824–8829.

[32] E. Sihite, X. Hu, B. Li, A. Salagame, P. Ghanem, and A. Ramezani, *Bang-Bang Control Of A Tail-less Morphing Wing Flight*, Issue: arXiv:2205.06395 arXiv: 2205.06395 [cs, eess], May 2022.

[33] P. Dangol and A. Ramezani, "Thruster-assisted legged robot control (Conference Presentation)," *Unmanned Systems Technology XXII*, vol. 11425, p. 1 142 507, 2020.

[34] P. Dangol, E. Sihite, and A. Ramezani, "Control of Thruster-Assisted, Bipedal Legged Locomotion of the Harpy Robot," *Frontiers in Robotics and AI*, vol. 8, 2021.

[35] P. Dangol and A. Ramezani, "Feedback design for Harpy: A test bed to inspect thruster-assisted legged locomotion," in *Unmanned Systems Technology XXII*, vol. 11425, SPIE, May 2020, pp. 49–55.

[36] P. Dangol and A. Ramezani, "Towards thruster-assisted bipedal locomotion for enhanced efficiency and robustness," *IFAC-PapersOnLine*, 21st IFAC World Congress, vol. 53, no. 2, pp. 10 019–10 024, Jan. 2020.

[37] K. Liang, E. Sihite, P. Dangol, A. Lessieur, and A. Ramezani, "Rough-Terrain Locomotion and Unilateral Contact Force Regulations With a Multi-Modal Legged Robot," in *2021 American Control Conference (ACC)*, May 2021, pp. 1762–1769.

[38] E. Sihite, P. Ghanem, A. Salagame, and A. Ramezani, "Unsteady aerodynamic modeling of Aerobat using lifting line theory and Wagner's function," in *2022 IEEE/RSJ International Conference on Intelligent Robots and Systems (IROS)*, Oct. 2022, pp. 10 493–10 500.

[39] E. Sihite, A. Ramezani, and M. Gharib, "Dynamic modeling of wing-assisted inclined running with a morphing multi-modal robot," in *2024 IEEE International Conference on Robotics and Automation (ICRA)*, May 2024, pp. 2339–2345.

[40] E. Sihite, P. Kelly, and A. Ramezani, *Mechanism Design of a Bio-inspired Armwing Mechanism for Mimicking Bat Flapping Gait*, Issue: arXiv:2010.04702 arXiv: 2010.04702 [cs], Oct. 2020.

[41] B. Gupta, A. Dhole, A. Salagame, *et al.*, "Bounding Flight Control of Dynamic Morphing Wings," in *2024 IEEE International Conference on Advanced Intelligent Mechatronics (AIM)*, Jul. 2024, pp. 100–105.

[42] B. Gupta, E. Sihite, and A. Ramezani, *Modeling and Controls of Fluid-Structure Interactions (FSI) in Dynamic Morphing Flight*, Issue: arXiv:2406.13039 arXiv: 2406.13039 [cs], Jun. 2024.

[43] A. Dhole, B. Gupta, A. Salagame, *et al.*, "Hovering Control of Flapping Wings in Tandem with Multi-Rotors," in *2023 IEEE/RSJ International Conference on Intelligent Robots and Systems (IROS)*, Oct. 2023, pp. 6639–6644.

[44] E. Sihite, F. Slezak, I. Mandralis, *et al.*, "Demonstrating Autonomous 3D Path Planning on a Novel Scalable UGV-UAV Morphing Robot," in *2023 IEEE/RSJ International Conference on Intelligent Robots and Systems (IROS)*, Oct. 2023, pp. 3064–3069.

[45] E. Sihite, B. Mottis, P. Ghanem, A. Ramezani, and M. Gharib, "Efficient Path Planning and Tracking for Multi-Modal Legged-Aerial Locomotion Using Integrated Probabilistic Road Maps (PRM) and Reference Governors (RG)," in *2022 IEEE 61st Conference on Decision and Control (CDC)*, Dec. 2022, pp. 764–770.

[46] K. Kim, P. Spieler, E.-S. Lupu, A. Ramezani, and S.-J. Chung, "A bipedal walking robot that can fly, slackline, and skateboard," *Science Robotics*, vol. 6, no. 59, eabf8136, Oct. 2021.

[47] A. Ramezani, P. Dangol, E. Sihite, A. Lessieur, and P. Kelly, "Generative Design of NU's Husky Carbon, A Morpho-Functional, Legged Robot," in *2021 IEEE International Conference on Robotics and Automation (ICRA)*, May 2021, pp. 4040–4046.

[48] A. Lessieur, E. Sihite, P. Dangol, A. Singhal, and A. Ramezani, "Mechanical design and fabrication of a kinetic sculpture with application to bioinspired drone design," in *Unmanned Systems Technology XXIII*, vol. 11758, SPIE, Apr. 2021, pp. 21–27.

[49] A. Salagame, M. Gianello, C. Wang, *et al.*, *Quadrupedal Locomotion Control On Inclined Surfaces Using Collocation Method*, Issue: arXiv:2312.08621 arXiv: 2312.08621 [cs, eess], Dec. 2023.

[50] A. Salagame, N. Bhattachan, A. Caetano, *et al.*, "How Strong a Kick Should be to Topple Northeastern's Tumbling Robot?" In *2024 IEEE International Conference on Advanced Intelligent Mechatronics (AIM)*, Jul. 2024, pp. 76–81.

[51] S. Jiang, A. Salagame, A. Ramezani, and L. L. S. Wong, "Snake Robot with Tactile Perception Navigates on Large-scale Challenging Terrain," in *2024 IEEE International Conference on Robotics and Automation (ICRA)*, May 2024, pp. 5090–5096.

[52] K. V. Krishnamurthy, E. Sihite, C. Wang, *et al.*, *Enabling steep slope walking on Husky using reduced order modeling and quadratic programming*, Issue: arXiv:2411.11788 arXiv: 2411.11788 [cs], Nov. 2024.

[53] K. V. Krishnamurthy, C. Wang, S. Pitroda, *et al.*, "Narrow-Path, Dynamic Walking Using Integrated Posture Manipulation and Thrust Vectoring," in *2024 IEEE International Conference on Advanced Intelligent Mechatronics (AIM)*, Jul. 2024, pp. 898–903.

[54] K. V. Krishnamurthy, C. Wang, S. Pitroda, *et al.*, *Thruster-Assisted Incline Walking*, arXiv:2406.13118 [cs], Jun. 2024.

[55] I. Mandralis, E. Sihite, A. Ramezani, and M. Gharib, "Minimum Time Trajectory Generation for Bounding Flight: Combining Posture Control and Thrust Vectoring," in *2023 European Control Conference (ECC)*, Jun. 2023, pp. 1–7.

[56] B. Gupta, Y. Shah, T. Liu, E. Sihite, and A. Ramezani, "Banking Turn of High-DOF Dynamic Morphing Wing Flight by Shifting Structure Response Using Optimization," in *2024 IEEE International Conference on Advanced Intelligent Mechatronics (AIM)*, Jul. 2024, pp. 94–99.

[57] A. Ramezani, M. Schroeter, I. McCarthy, and A. Salagame, "Crater observing bio-inspired rolling articulator," 20240317336A1, Type: patentus, Sep. 2024.

[58] S. Pitroda, A. Bondada, K. Venkatesh, *et al.*, "Capture Point Control in Thruster-Assisted Bipedal Locomotion," in *2024 IEEE International Conference on Advanced Intelligent Mechatronics (AIM)*, Jul. 2024, pp. 1139–1144.

[59] E. Sihite, A. Kalantari, R. Nemovi, A. Ramezani, and M. Gharib, "Multi-Modal Mobility Morphobot (M4) with appendage repurposing for locomotion plasticity enhancement," *Nat Commun*, vol. 14, no. 1, p. 3323, Jun. 2023.

[60] A. Ramezani and K. Sreenath, "Thruster-Assisted Legged Mobility for Explorations on Mars," vol. 2655, p. 5074, Mar. 2022.

[61] A. Ramezani, E. Sihite, S. Devey, and M. Gharib, "Efficient and Endured Aerial Mobility on Mars Using Novel Morphing Micro Aerial Vehicle Designs," vol. 2655, p. 5051, Mar. 2022.

[62] A. Ramezani, "Towards biomimicry of a bat-style perching maneuver on structures: The manipulation of inertial dynamics," in *2020 IEEE International Conference on Robotics and Automation (ICRA)*, May 2020, pp. 7015–7021.

[63] V. Riviere, A. Manecy, and S. Viollet, "Agile Robotic Fliers: A Morphing-Based Approach," *Soft Robotics*, vol. 5, no. 5, pp. 541–553, Oct. 2018, Publisher: Mary Ann Liebert, Inc., publishers.

[64] S. Ryu, Y. Lee, and T. Seo, "Shape-Morphing Wheel Design and Analysis for Step Climbing in High Speed Locomotion," *IEEE Robotics and Automation Letters*, vol. 5, no. 2, pp. 1977–1982, Apr. 2020.

[65] X. Zhang, F. Zhou, X. Xu, T. Zou, and H. Chen, "Configuration Design and Analysis of a Multimodal Wheel with Deformable Rim," in *2019 IEEE/ASME International Conference on Advanced Intelligent Mechatronics (AIM)*, ISSN: 2159-6255, Jul. 2019, pp. 772–777.

[66] L. Daler, S. Mintchev, C. Stefanini, and D. Floreano, "A bioinspired multi-modal flying and walking robot," en, *Bioinspiration & Biomimetics*, vol. 10, no. 1, p. 016 005, Jan. 2015, Publisher: IOP Publishing.

[67] B. Araki, J. Strang, S. Pohorecky, C. Qiu, T. Naegeli, and D. Rus, "Multi-robot path planning for a swarm of robots that can both fly and drive," in *2017 IEEE International Conference on Robotics and Automation (ICRA)*, 2017-05, pp. 5575–5582.

[68] K. Peterson, P. Birkmeyer, R. Dudley, and R. S. Fearing, "A wing-assisted running robot and implications for avian flight evolution," en, *Bioinspiration &amp$\mathsemicolon$ Biomimetics*, vol. 6, no. 4, p. 046 008, Oct. 2011, Number: 4 Publisher: IOP Publishing.

[69] R. J. Bachmann, R. Vaidyanathan, F. J. Boria, *et al.*, "A Miniature Vehicle with Extended Aerial and Terrestrial Mobility," en, in *Flying Insects and Robots*, Springer, Berlin, Heidelberg, 2009, pp. 247–270.

[70] A. Kalantari and M. Spenko, "Design and experimental validation of HyTAQ, a Hybrid Terrestrial and Aerial Quadrotor," in *2013 IEEE International Conference on Robotics and Automation*, ISSN: 1050-4729, May 2013, pp. 4445–4450.

[71] R. Baines, S. K. Patiballa, J. Booth, *et al.*, "Multi-environment robotic transitions through adaptive morphogenesis," en, *Nature*, vol. 610, no. 7931, pp. 283–289, Oct. 2022, Publisher: Nature Publishing Group.

[72] M. Bjelonic, P. K. Sankar, C. D. Bellicoso, H. Vallery, and M. Hutter, "Rolling in the Deep – Hybrid Locomotion for Wheeled-Legged Robots Using Online Trajectory Optimization," *IEEE Robotics and Automation Letters*, vol. 5, no. 2, pp. 3626–3633, Apr. 2020.

[73] Simplify3D. "Filament properties table." (), [Online]. Available: `https://www.simplify3d.com/resources/materials-guide/properties-table/`.